Materials Today Communications 16 (2018) 152–163

Contents lists available at ScienceDirect

Materials Today Communications

journal homepage: www.elsevier.com/locate/mtcomm

Nanostructured hydroxyapatite networks: Synergy of physical and chemical cues to induce an osteogenic fate in an additive-free medium

J. Sartuqui[a,*], C. Gardin[b], L. Ferroni[b], B. Zavan[b], P.V. Messina[a]

[a] Department of Chemistry, Universidad Nacional del Sur, INQUISUR-CONICET, 8000 Bahía Blanca, Argentina
[b] Department of Biomedical Sciences, University of Padova, via U. Bassi 58/B, 35131 Padova, Italy

ARTICLE INFO

Keywords:
Hydroxyapatite networks
Osteogenic differentiation
Adipose derived stem cells
Additive free medium

ABSTRACT

Nanoscale topography plays a central role in adult-stem-cell-niches. In this study we have demonstrated that by an accurate material design, mimicking the composition and structure of bone extracellular matrix, it is possible to guide human adipose stem cells (hASCs) to attain an osteogenic commitment, *in vitro,* without the requirement of soluble additives or grow factors. Alkaline Phosphatase (ALP) activity and Alizarin Red S test demonstrated that hASCs cultured onto hydroxyapatite frameworks dry-coating differentiated into mature osteoblasts even in the absence of specific inducing factors. Optical and electron scanning microscopic (SEM) observations revealed a direct cellular-material interaction that indicated an appropriate communication between nanotopographical features and the integrin receptors in the cell´s focal adhesions. Real-time quantitative PCR (RT-qPCR) analysis confirmed the expression of specific markers of pre-osteoblast and mature osteoblast stages as osterix (OSX), osteopontin (OPN), osteocalcin (OC) and; specific markers of extracellular matrix maturation and mineralization stages as alkaline phosphatase (ALPL), collagen type I alpha 1 (COL1A1) and osteonectin (ON). Osteoprotegerin (OPG), ALPL, COL1A1, and sclerostin (SOST) expressions were up regulated compared to osteogenic differentiation media conditions.

1. Introduction

Bone defects represent a challenge for the clinical field as a result of the difficulties in restoring its biological function by simply repair or replacement [1,2]. Therefore, there is a great demand of new alternatives intended to the induction of its regeneration. One of them are the so called bone bioreactors, wherein autologous harvested cells are seeded into a synthetic scaffold and stimulated with exogenous mitogens and morphogens, *in vitro* and/or *in vivo*[3], to attain a healing response within the bioreactor space. Under this approach the key point to achieve an efficient bioreactor is the scaffold device. On basis of the biomimicry principle that focuses on the creation of a natural scenery triggering the cells to do what they do best [4], a hypothetical tactic is the construction of an effective scaffold material reproducing both chemical and morphological characteristics of osteogenic niches [5] to activate the necessary chemotactic factors to promote the desired cellular responses and the ensuing regeneration of healthy tissue. Thereby, through an accurate material design, reportedly, displaying nanoscale features [6–8], it is possible to capitalize the cells' innate abilities to respond to their environment without the requirement of genetic or pharmacological manipulations. In previous works [9–11] we have synthesized, characterized and proved the *in vitro* bone regeneration potential of biodegradable nanostructured frameworks obtained by the assembly of hydroxyapatite (HA) nano-rods; their features result from their osteoconductive micro environmental skills comparable to those of bone extracellular matrix (ECM). Here we demonstrate the *in vitro* ability of the prepared materials to induce an effective substrate stimulus to drive the osteogenic differentiation and mineralization of human adipose-derived stem cells (hASCs) in the absence of selective sera lots or soluble growth factor supplements. Human ASCs are a mesenchymal stem cell source with self-renewal ability and a multipotential differentiation. They are easier to collect, isolate and culture than bone-marrow derived mesenchymal stem cells (BMSCs) [12], and have no ethical or political issues compared to embryonic stem cells (ESCs) [13]. These characteristics make hASCs an acceptable solution for tissue regenerative approaches. Existing reports and clinical trials point out that hASCs in 3D scaffolds could be a potential alternative for wound healing [14], cardiovascular grafts [15], orthopedic tissue repair [16], oral and maxillofacial tissue engineering [17] and plastic tissue reconstruction after surgery [18]. The goal in the present study was to show the possibility to exploit the HA nano-rods superstructures - hASCs systems as bone tissue bioreactors. The HA nanostructured

* Corresponding author.
E-mail address: jsartuqui@inquisur-conicet.gob.ar (J. Sartuqui).

https://doi.org/10.1016/j.mtcomm.2018.05.010
Received 7 February 2018; Received in revised form 24 April 2018; Accepted 25 May 2018
Available online 26 May 2018
2352-4928/ © 2018 Elsevier Ltd. All rights reserved.

matrix offer, simultaneously, physical support and a biologically active environment for the attachment, survival and osteo-differentiation of hASCs inducing the progression of a new mineral matrix. The obtained results would contribute to the development of new bone tissue engineering strategies inspired by the endogenous bone healing mechanisms.

2. Experimental

2.1. Reagents

Hexadecyl-trimethyl ammonium bromide (CTAB, MW = 364.48 g / mol, 99% Sigma-Aldrich); poly(ethylene glycol) 400 (PEG 400, Sigma-Aldrich, MW = 380–420 g / mol, δ = 1.126 g / mL at 25 °C); poly (propylene glycol) (PPG, Sigma-Aldrich, MW = 425 g / mol, δ = 1.004 g / mL at 25 °C); sodium phosphate (Na_3PO_4, MW = 148 g / mol, 96% Sigma-Aldrich); calcium chloride ($CaCl_2$, MW = 110.9 g / mol, 99% Sigma-Aldrich); sodium nitrite ($NaNO_2$, MW = 69 g / mol, 97% Sigma-Aldrich); dimethyl sulfoxide (DMSO, MW = 78.13 g / mol, δ = 1,1 g / mL at 25 °C, 99% Sigma-Aldrich); isopropyl alcohol (IprOH, MW = 60.10 g / mol, δ = 078 g / mL at 25 °C, 99.5% Sigma-Aldrich); ethanol (EtOH, MW = 46.07 g / mol, δ = 078 g / mL at 25 °C, 96% Sigma-Aldrich); paraformaldehyde (PFA, MW = 30.03 g / mol (as monomer), Sigma-Aldrich) were used without further purification. 3-(4,5-Dimethylthiazol-2-yl)-2,5-Diphenyltetrazolium Bromide (MTT, Sigma-Aldrich, 5 mg / mL); phosphate buffered saline (PBS without Ca/Mg, EuroClone, Milan, Italy); Trypsin-EDTA solution (trypsin/EDTA, EuroClone, Milan, Italy); Alizarin Red S Solution (ARS, Sigma-Aldrich). Complete Dulbecco's Modified Eagle's Medium (cDMEM) was made of Dulbecco's modified Eagle's medium (DMEM, Lonza S.r.*l.*, Milano, Italy) supplemented with 10% Fetal Bovine Serum (FBS, Bidachem S.p.A., Milano, Italy) and 1% Penicillin/Streptomycin (P/S, EuroClone). Osteogenic differentiation medium (ODM) was composed of cDMEM supplemented with 10 ng / mL Fibroblast Growth Factor 2 (FGF-2, ProSpec, East Brunswick, NJ, USA), 10 mM β-glycerophosphate (Sigma-Aldrich), and 10 nM dexamethasone (Sigma-Aldrich). SEM fixation solution: 2.5% glutaraldehyde (GA) in 0.1 M cacodylate (CAC) buffer (2.5% GA -0.1 M CAC, Poly Scientific R *E* D Corp., USA). Alkaline Phosphatase Assay activity kit (ALP kit, Abcam, ab83369). For total RNA (tRNA), complementary DNA (cDNA) isolation and real-time PCR (r–t PCR) procedures Total RNA Purification Plus Kit (tRNA - ppKit, Norgen Biotek Corp., Thorold, ON, Canada); SensiFAST™ cDNA Synthesis Kit (sFAST™- cDNAsKit, Bioline, London, UK) and SensiFAST™ SYBR No-ROX Kit (sFAST™ – sNorKit, Bioline, London, UK) were used. For solutions preparation, only sterile Milli-Q® water was used. For all experiments passage two (P2) cells were used.

2.2. Nanostructured HA-framework dispersion

Nanostructured frameworks were obtained by the assembly of HA nano-rods of 8 ± 1 nm diameters and 28 ± 3 nm length by a previously described methodology. [9] Two HA nano-rod materials templated by CTAB-PPG and CTAB-PEG-400 aqueous structured networks and denoted as MI and MII respectively are evaluated. The synergistic interaction of each block copolymer in contact with CTAB rod-like micelles results in hierarchically organized structures exhibiting different micro-rough characteristics [9,10]. Prior to use, both samples were sterilized in an autoclave at 120 °C during 30 min. Then a sterile Milli-Q® water material (71.42 µg / mL) dispersion was prepared by placing the components on a rotating mixer for 5 min.

2.3. Nanostructured HA-frameworks dry-coatings

A 24-well plate (2 cm^2 / well), flat bottom, was filled with the properly amount of Milli-Q® water material dispersion to have a final cytocompatible level of nano-HA coating of 60 µg/cm^2 [10]. The material-coatings were allowed to dry overnight on shaker in a biological safety cabinet to obtain a homogeneous dry-coat surface on the bottom of the well. For scanning electronic microscopy (SEM) and Alizarin Red S assays, MI and MII dry-coatings were prepared on 1.2 cm diameter round coverslips placed on each well. When it was required half of the coverslips were cover with material dry-coating, for this a half of the glass coverslip was protected with laboratory film (P7793 SIGMA PARAFILM® M roll size 4 in. × 125 ft) before material deposition; the film was removed after the coating process. The homogeneous distribution and attachment of HA nano-material on dry-coatings was checked by optical microscopy (Leica DM IRB).

2.4. Isolation of ASCs from human adipose tissue and culture

Human ASCs were isolated from the adipose tissue of healthy patients (age: 21–36 years; body mass index (BMI): 30–38) undergoing cosmetic surgery procedures according to the guidelines of the plastic surgery clinic at the University of Padova, Italy. Before their inclusion in this study, written informed consent was obtained from all patients, in accordance with the Helsinki Declaration. The adipose tissues were digested and the cells isolated and expanded as previously described. [19] At confluence, hASCs at passage two (P2) were harvested by trypsin-EDTA solution treatment.

2.5. Human ASCs seeded on nanostructured HA-frameworks dry-coatings

Simultaneous batches of hASCs cultured at a density of 3 × 10^4 cells / cm^2 in a 24-well plate, flat bottom, either in ODM and cDMEM on HA-frameworks dry-coatings were analyzed up to 21 days of treatment to ensure differentiation stability. [20,21] The culture medium was changed twice a week. Experiments were performed with three different cell preparations and repeated three times.

2.6. Mitochondrial metabolic activity and viability assays

The viability of hASCs seeded onto MI and MII dry-coatings was evaluated after 7 and 21 days of culture in cDMEM or in ODM using the MTT-based cytotoxicity assay, as described in Denizot and Lang. [22] Viable hASCs with active metabolism reduce MTT into a purple colored formazan product that can be solubilized and quantified by spectrophotometric means. When cells die, they lose the ability to convert MTT into formazan, thus color formation serves as a marker of only metabolically active cells. [23,24] Therefore, this assay was performed with the objective to evaluate the hASCs metabolic activity and indirectly their viability when cultured with the nano-HA materials. [24] After the culture period (7 or 21 days), cells were incubated with 1 mL of 0.5 mg / mL MTT-PBS solution for 3 h at 37 °C under humidified air (5% CO_2). Next MTT-PBS solution was removed and each sample was extracted with 0.5 mL of 10% DMSO in IprOH solution for 30 min at 37 °C. For each sample, 200 µL aliquots, in duplicate, were used for optical density (OD) recordings at 570 nm by means of a multilabel plate reader (Victor 3, PerkinElmer, Milano, Italy). The absorbance of coated wells without cells was used as blanks.

2.7. Analysis of hASCs growth and morphology: localization, spreading and attachment

The homogeneous distribution and attachment of HA nano-material on the bottom of the wells after hASCs seeding was checked by optical microscopy (Leica DM IRB). Cells cultured on uncoated wells were used as control (C).

Table 1
List of genes and human primer sequences used in the r–t PCRs study.

Gene		Primer base sequence (5'- 3')	
Symbol	Function	Forward	Reverse
Skeletal Development			
ALPL	Ossification	GGCTTCTTCTTGCTGGTGGA	CAAATGTGAAGACGTGGGAATGG
OC		GCAGCGAGGTAGTGAAGAGAC	AGCAGAGCGACACCCTA
ON		TGCATGTGTCTTAGTCTTAGTCACC	GCTAACTTAGTGCTTACAGGAACCA
OPG		AAACGCAGAGAGTGTAGAGAGG	TCGAAGGTGAGGTTAGCATGTC
OPN		TGGAAAGCGAGGAGTTGAATGG	GCTCATTGCTCTCATCATTGGC
RUNX2		AGCCTTACCAAACAACACAACAG	CCATATGTCCTCTCAGCTCAGC
COL1A1	Extracellular (ECM) matrix molecules	TGAGCCAGCAGATCGAGA	ACCAGTCTCCATGTTGCAGA
Cell Differentiation and Growth			
BMP2	BMP Receptor Signaling	CCACTAATCATGCCATTGTTCAGAC	CTGTACTAGCGACACCCACAA
OSX	Osteoblast differentiation	TCAGAATCTCAGTTGATAGGGTTTCTC	GGGTACATTCCAGTCCTTCTCC
RANKL	Osteoclast genesis	TCAGCATCGAGGTCTCCAAC	CCATGCCTCTTAGTAGTCTCACA
SOST	Bone formation regulation	TGTGGTTTCTAGTCCTGGCTC	TTCTCTCTCTCTCTCTCACCTCTG
FGF-2	Angiogenesis	5′-GGCTTCTTCCTGCGCATCCA-3'	5′-GCTCTTAGCAGACATTGGAAGA-3′
Housekeeping gene			
TFRC		TGTTTGTCATAGGGCAGTTGGAA	ACACCCGAACCAGGAATCTC

ALPL, alkaline phosphatase, liver/bone/kidney; BMP2, bone morphogenetic protein 2; COL1A1, collagen, type I, alpha 1; OC, osteocalcin; ON, osteonectin; OPG, osteoprotegerin; OPN, osteopontin; OSX, osterix; RANKL, receptor activator of nuclear factor kappa-B ligand; RUNX2, runt-related transcription factor 2; SOST, sclerostin; TFRC, transferrin receptor; FGF-2, fibroblast growth factor.

3. Human ASCs osteogenic differentiation and mineralization

3.1. Alkaline phosphatase (ALP) activity measurements

The intracellular ALP activity of hASCs seeded onto MI and MII dry-coatings and cultured during 7 and 21 days either in cDMEM or in ODM was measured using a colorimetric ALP kit. According to the manufacturer protocol, cells on powders were washed with PBS, homogenized with the ALP Assay Buffer (300 µL in total for each group) and finally centrifuged at 13,000 rpm for 3 min to remove insoluble material. Different volumes of samples were then added into 96-well plates, bringing the total volume in each well up to 80 µL with ALP Assay Buffer. Thereafter, 50 µL of 5 mM p-nitrophenyl phosphate (pNPP) substrate solution was added to each well containing the test samples and incubated for 60 min at 25 °C, protecting the plate from the light. A standard curve of 0, 4, 6, 12, 16, and 20 nmol / well was generated from 1 mM pNPP standard solution bringing the final volume to 120 µL with ALP Assay Buffer. After stopping all reactions with 20 µL of Stop solution, optical density (OD) values were recorded at λ_{max} = 405 nm in a microplate reader (Victor 3, Perkin Elmer, Milano, Italy). The results were normalized subtracting the value derived from the zero standards from all standards and samples. The pNPP standard curve was plotted to identify the pNPP concentration in each sample. ALP activity of the test samples was calculated as follows:

$$ALP_{activity}\left(\frac{U}{mL}\right) = \frac{A/V}{T}$$

where A is the amount of pNPP generated by samples (in µmol), V is the amount of sample added in the assay well (in mL), and T is the reaction times (in minutes).

3.2. Alizarin red S staining

The extracellular mineral deposits were detected by Alizarin Red S staining. Cells grown onto MI and MII dry-coatings after cultured for 7 and 21 days either in cDMEM or in ODM were fixed in 4% PFA in PBS solution for 10 min at room temperature (RT). Cells were stained adding 40 mM freshly ARS Solution, pH 4.2, for 10 min at RT with gentle shaking. Cells were washed with sterile Milli-Q® water, and then examined by an optical microscope (Leica DM4000 M).

3.3. Human ASCs micro-morphology observation

For the microscopic analysis of hASCs' micromorphology after the interaction with nano-HA materials, hASCs were seeded onto MI and MII dry coatings (Section 2.3) and then cultured during 7 and 21 days either in cDMEM or in ODM. At the end of the incubation period they were fixed with 2.5% GA - 0.1 M CAC for 1 h and then progressively dehydrated in EtOH accordingly to biological samples' SEM fixation protocols. [25] Specimens were fixed on carbon double-side tape with silver paste, coated with gold alloy (Edwards S150A, sputter coating unit, Edwards, Crawley, UK) and observed with a SEM (JEOL JSM-6490LV, JEOL, Tokio, Japan) provided by the Interdepartmental Service Center CEASC (Centro di Analisi e Servizi Per la Certificazione, University of Padova, Italy). The associated X-ray fluorescence microanalysis provided qualitative information about surface elemental composition.

3.4. Quantitation of RNAs from specific genes: total RNA isolation and real-time PCR procedure

To confirm the osteogenic induction, tRNA was isolated with a tRNA-ppKit from hASCs seeded onto MI and MII dry-coatings and incubated for 7 and 21 days either in cDMEM or in ODM. NanoDropTM ND-1000 (Thermo Fisher Scientific, Waltham, MA, USA) was used to assess quality and concentration of the RNA samples. cDNA was obtained from 500 ng of total RNA using a sFAST™-cDNAsKit following the manufacturer's protocol. r–t PCRs were performed on a Rotor-Gene 3000 (Corbett Research, Sydney, Australia) using the sFAST™ – sNorKit and 400 nM concentration of the designed primers provided by the Kit. Values were normalized to the expression of the transferrin receptor (TFRC) housekeeping gene, and differences in gene expression were evaluated by the 2ΔΔCt method [26]. Human primer sequences are detailed in Table 1.

3.5. Statistical analysis

All quantitative tests were carried out at least in triplicate, and then mean values with standard deviations were calculated. Statistical analysis of data was accomplished by one factor analysis of variance (ANOVA). Student's *t*-test and probability values below 0.05, ($p < 0.05$) were considered significantly different. Quantitative data are expressed as mean ± standard deviation (SD) from the indicated set of

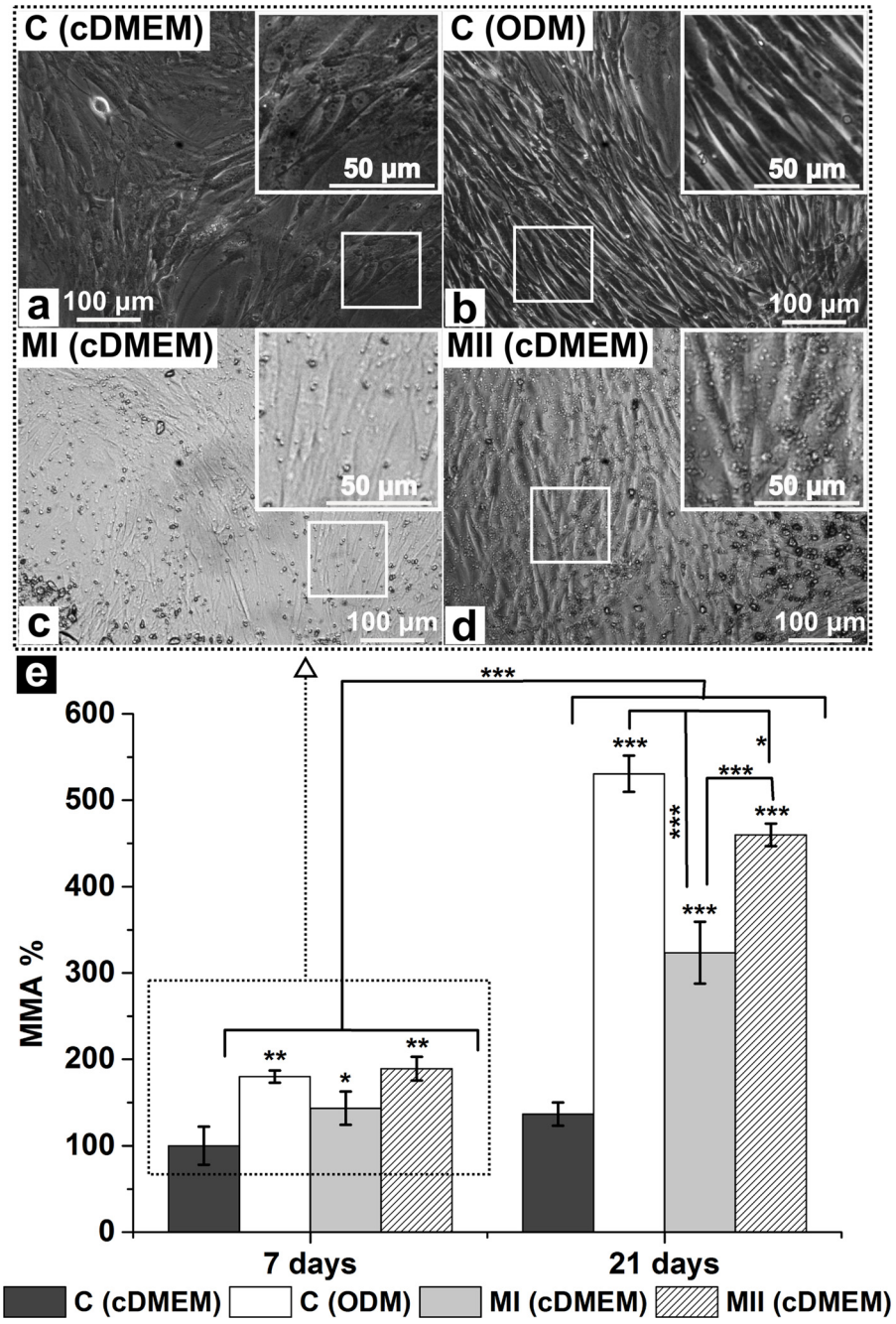

Fig. 1. Optical microscopic images of hASCs adhered on: (a, b) non-coated glass coverslips after 7 days of culture either in cDMEM or ODM and; (c, d) 60 µg/cm^2 nanostructured HA-frameworks dry-coatings (MI and MII) after 7 days of culture in cDMEM. (e) Mitochondrial metabolic activity (MMA) of hASCs adhered on 60 µg/cm^2 nanostructured HA-frameworks dry-coatings (MI and MII) after 7 and 21 days of culture in cDMEM. MMA data are normalized to cells performance after 7 days of culture in cDMEM without the presence of nano-HA; asterisks denote statistically significant differences (*$p < 0.05$, **$p < 0.01$ and ***$p < 0.001$). Significant differences between the samples are indicated with brackets. Cells cultured on uncoated wells in both cDMEM and ODM were used as controls (C).

experiments.

4. Results

4.1. Attachment, survival and distribution of hASCs on nanostructured HA-Frameworks dry-coatings

To account the biological effects of the manufactured materials, in pursuit of their clinically relevant requirements to be used as a cellular support, [27,28] the first step was to assess the viability and metabolic activity of hASCs as a way to test the materials' capacity to assist initial cell spreading and proliferation, results are shown in Fig. 1a–e.

Cells cultured on both ODM and cDMEM rapidly adhered to attain a confluent monolayer onto the HA-frameworks dry-coatings and were found completely organized after 7 days of seeded; no morphological statistical significant differences can be appreciated compared with controls, meaning the cells were viable, Fig. 1a–d. Both in ODM and in the presence of MI and MII samples, Fig. 1b–d, an increase in cells' proliferation was evidenced validating the obtained mitochondrial metabolic activity (MMA) values, Fig. 1e. A clear influence of culture media on the hASCs' MMA was noticed. Cells cultured on uncoated wells in cDMEM exhibited a no statistically significant increase of MMA throughout the treatment progression (21 days) which it is definite detected when they were cultured in ODM, Fig. 1e. Nanostructured HA-frameworks does not significantly affect the cellular MMA in ODM; **Fig. SI1** of supporting information (**SI**). However in cDMEM there is a statistically significant increase of hASCs' MMA from the earliest 7 days of treatment, Fig. 1e; a superior effect was detected for cells cultured onto MII dry-coating. No statistically significant differences can be detected between the hASCs' MMA after 21 days of adhesion on MII dry-coating whether they were cultured in ODM or in cDMEM, **Fig. SI2**. This information evidenced a clear regulation of MII sample on the cells' MMA

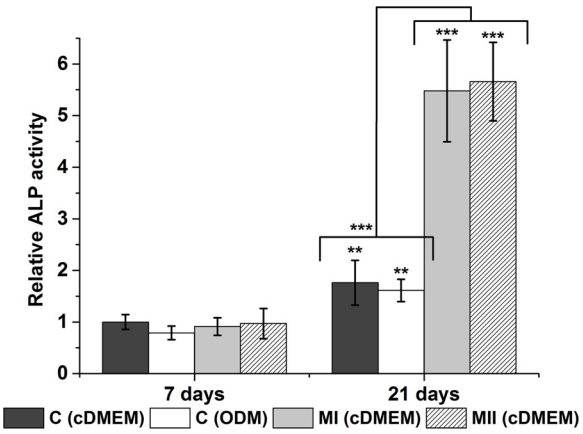

Fig. 2. Alkaline Phosphatase (ALP) activity of hASCs adhered on 60 μg/cm^2 nanostructured HA-frameworks dry-coatings after 7 and 21 days of culture in cDMEM. Data are normalized to cells performance after 7 days of culture in cDMEM without the presence of nano-HA. Asterisks denote statistically significant differences (*$p < 0.05$, **$p < 0.01$ and ***$p < 0.001$), significant differences between the samples are indicated with brackets. Cells cultured on uncoated wells in both cDMEM and ODM were used as controls (C).

which is equivalent to that attained in the presence of soluble osteogenic additives. In view of the materials' ability to induce a hASCs' MMA and viability in cDMEM similar to that observed under osteogenic soluble additives effect, the next step was to evaluate their influence to drive hASCs commitment.

4.2. hASCs – nanostructured HA substrate interactions

The hASCs' inductions toward osteogenic commitment were characterized by the alkaline phosphatase (ALP) activity that it is a well-known differentiation marker, [21] results are shown in Fig. 2. After 7 days of culture in cDMEM, no statistically significant differences respect to controls were observed on the ALP activity of hASCs spread on HA-frameworks dry-coatings. The appreciated low ALP levels are consistent with initial actively proliferating cells committed to the osteoblast lineage, [29] that was confirmed by optical microscopic observation, Fig. 3a–c; g–i; m–o; s–u. A similar statistically significant increase ($p < 0.01$) on ALP activity was appreciated after 21 days of culture on uncoated wells, independently of the culture media. Statistically comparable values of ALP activity were obtained for cells cultured on HA-frameworks dry-coatings in ODM, without appreciation of any effect due to the presence of the material in this medium, **Fig. SI3**.

The obtained ALP activity values are indicative of the cessation of replication that marks the onset of differentiation [29,30] ; again this fact was confirmed by optical microscopy, Fig. 3d; j; p–r; v–x. Surprisingly, when hASCs were cultured on HA-frameworks dry-coatings throughout 21 days in cDMEM, a highly significant increase in ALP activity was found demonstrating that in such conditions hASCs can attain their maximum maturation capacity [29,30] and, that is superior than the achieved in the presence of soluble osteogenic inducing additives. Alizarin Red S staining was used to confirm the presence of mineralized matrix, since it specifically binds to highly enriched calcium deposits. [21] Being the substrates' chemical composition based on Ca-P, dye can also attach to it and give us a false positive. In order to distinguish the intracellular deposits of calcium from the apatitic substrate, we stained the HA-frameworks dry-coatings without cells addition to observe its morphology and coloration, **Fig. SI4**. The substrate is homogeneously distributed and stained in red, while its shape is considerably different from that of the deposits generated during hASCs' differentiation. The rectangular faceted shapes of the HA crystals are clearly appreciated and their coloration is semitransparent. On the other hand the cells' generated deposits are characterized by a dense red color and its form is almost circular denoting their origin from a nucleation center and growing outward in a radial arrangement. Examples of calcium stores in hASCs extracellular matrix, in all culture conditions, were shown in Fig. 3. No extracellular mineralized matrix clusters were observed over the 21 days of treatment when hASCs are cultured in cDMEM on non-coated glass coverslips, while internal reddish coloration detected may be associated to the beginning of the intracellular mineralization process, Figs. 3a, g, d, j, SI5a and SI5b. A significant increase in the number of cells compared to those cultured in cDMEM was observed for hASCs treated in ODM, Fig. 3m and s; formation of calcium deposits were seen only after 21 days of culture, Fig. 3p and v. In those conditions cells displayed elongated spindle morphology with abundant cytoplasm and large nuclei organized in parallel, Figs. 3p, **v**, **SI5c** and **SI5d**. When hASCs were cultured on HA-frameworks dry-coatings in cDMEM, clusters of Ca-P deposits were observed since the first time point considered in the treatment, Fig. 3b, c, h and i; larger Ca-P deposits are formed on MII dry-coating, Fig. 3c and i. It was observed that hASCs interact directly with the HA-framework and organized in bundles around it; the new calcium deposits grow radially from the material that act as a nucleation center, **Figs. SI6a** and **SI6b**. In ODM, after 7 days of culture, the cells lose their characteristic parallel alignment; examples are shown in **Figs. SI6c** and **SI6d**. To corroborate the cell attraction for HA-nanostructures and the material's effect on their evolution beyond the ODM influence, a half coated glass coverslips was used; it was observed that after 7 days of treatment calcium deposits were developed in the area covered by the material, **Fig. SI7.** At 21 days of treatment, for cells cultured in either cDMEM or ODM, the materials' presence induced a significant development of ECM and Ca-P deposits, Fig. 3d, f, k, l, q, r, w and x. Nevertheless, during the ODM culture, hASCs increased their density and returned to their usual parallel alignment, calcium deposits remained disseminated, Fig. 3q, w, r and x. In addition, it was observed that cells spread on MII dry-coating and cultured in cDMEM have a larger area of extension showing the characteristic high-adhesion star morphology, **Figs. SI8a and SI8b**. Hence, the obtained results of ALP activity test and Alizarin Red S staining demonstrate that HA-frameworks dry-coatings *per se* are able to induce the hASCs osteogenic differentiation *in vitro* in absence of soluble osteogenic additives and that the rate and strength of this process is superior of that achieved in ODM.

The cell-substrate interaction was deeply evaluated by SEM microphotographs inspection. It can be observed that cells attached on HA-frameworks dry-coatings either cultured in cDMEM or in ODM, nevertheless such adhesion depend on the culture media and on the cellular fate evolution. After 7 days of culture, the surface was almost covered by cells and no significant differences relatives to the culture media can be appreciate, **figures SI9** and **SI10**. After 21 days of treatment, complete cell coverage was attained and cells overlapped showing 3-dimensional (3D) structures, which enable communication with each other, Figs. 4a and Figure a. As previously inferred, cells cultured in cDMEM interact directly with the material, Fig. 4a–c. High-magnification SEM images, Fig. 4d–f, revealed the presence of numerous hASCs extensions, filopods, protruding and anchorages direct to the nanostructure HA surface. Granular material forming concentric accumulations was also observed; Fig. 4f, fluorescence X-ray microanalysis confirmed that it is composed by mineralized matrix components. Optical and SEM microphotographs analysis evidenced a high number of specific features (flat and extended bodies, extracellular calcium deposits) that confirmed that cells spread on HA-frameworks dry-coatings and cultured in cDMEM acquiring the typical osteoblastic feature. Unlike cell cultured in cDMEM a parallel cell alignment occurred in ODM; in such conditions no specific cell-material interactions were observed, Fig. 5a–d.

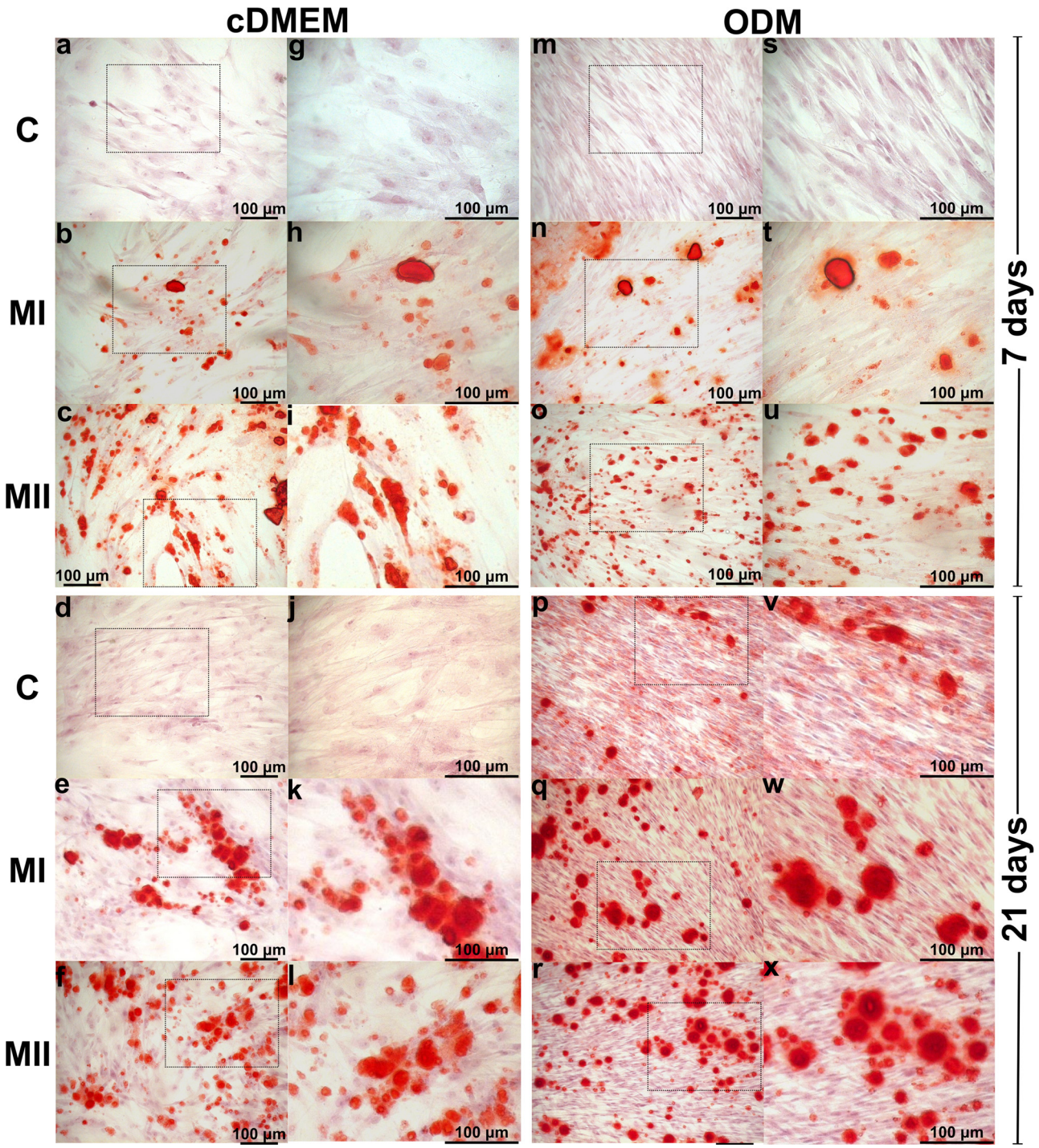

Fig. 3. Alizarin Red S staining of hASCs adhered on 60 µg/cm2 nanostructured HA-frameworks dry-coatings cultured throughout 7 and 21 days in cDMEM and ODM; optical microphotographs (a–f, m–r) 20 x magnification and (g–l, s–x) 40 x magnification. Cells cultured on non-coated glass coverslips in both cDMEM and ODM were used as control (C).

4.3. expression of mRNA related to osteogenesis: progressive Gene expression profiles

To further evaluate the effect of HA-frameworks on the osteogenic commitment, gene expressions for osteogenic differentiation were analyzed. The following osteogenic-specific markers associated to the skeletal development and the regulation of cell's evolution were considered: osteocalcin (OC), an osteoblast specific gene [31] associated to bone mineralization and calcium homeostasis [32]; osteonectin (ON), a calcium-binding glycoprotein secreted by osteoblasts during bone formation, it presence promote mineralization [33]; osteopontin (OPN), an extracellular structural protein, biosynthesized by osteoblast and involved in the cell attachment to the mineralized bone matrix [34]; osteoprotegerin (OPG), an excretory protein produced by evolving osteoblasts, its presence prevent bone resorption and enhance the synthesis bone matrix [35]; runt-related transcription factor 2 (RUNX2), it has a crucial role in the early determination stage of the osteoblast lineage [36]; alkaline phosphatase tissue non-specific isoenzyme (ALPL), a membrane-bound glycosylated enzyme that may act as an early indicator of cellular activity and osteoblast differentiation

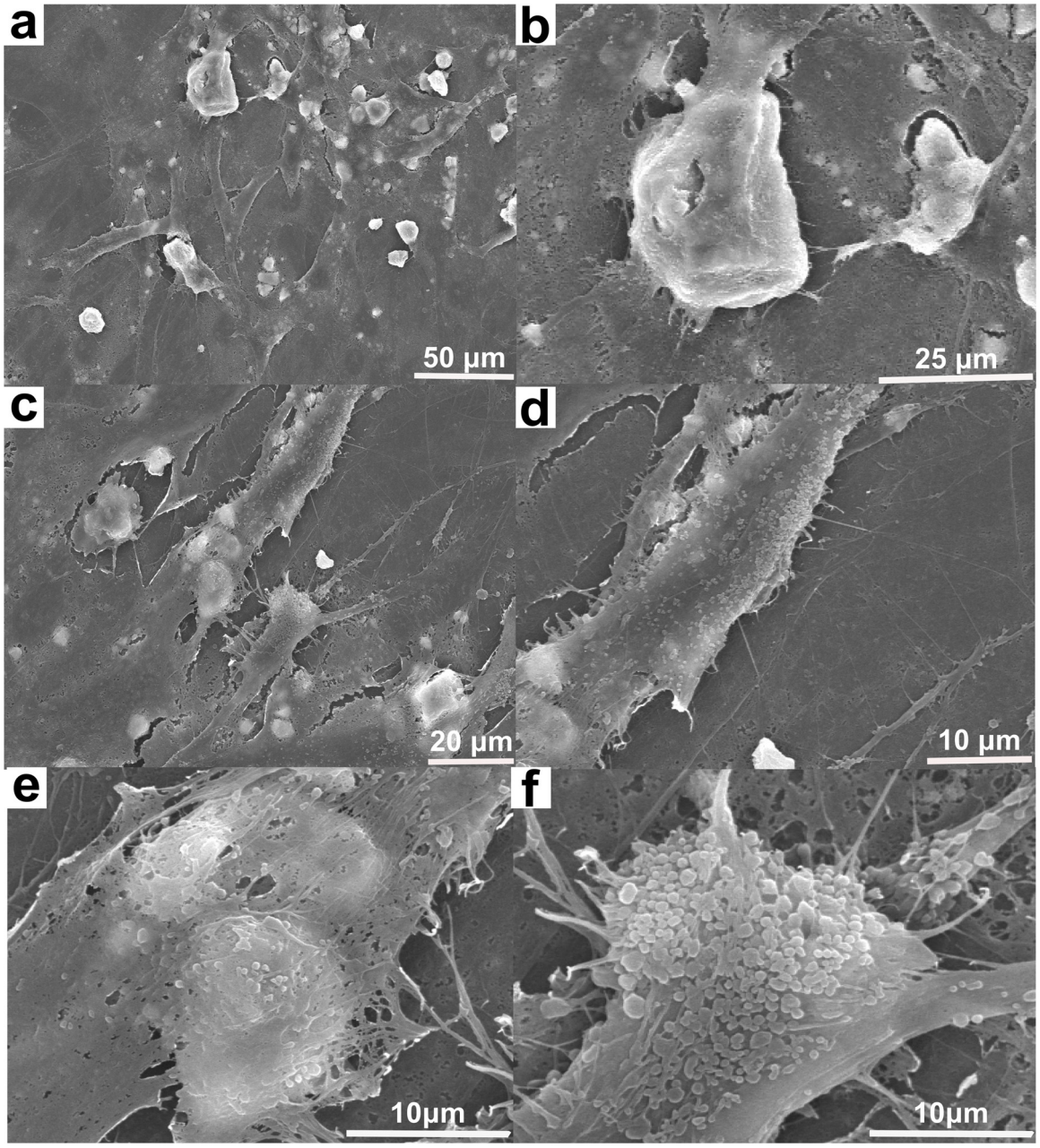

Fig. 4. SEM microphotographs of hASCs adhered on 60 µg/cm^2 nanostructured MII dry-coating cultured throughout 21 days in cDMEM.

[37]; collagen type I alpha 1 (COL1A1), a significant constituent of bone ECM establishing connections with cell surface integrins and other ECM proteins [38]; bone morphogenetic proteins-2 (BMP2), expressed by osteoprogenitor cells, it can stimulate the differentiation of osteoblast and can also mediate the expression of OSX in mesenchymal cells independent of the RUNX2′s regulation [39]; osterix (OSX), a typified osteoblast specific gene [40], regulates the later stage of osteoblast differentiation and bone formation [36]; receptor activator of nuclear factor κ-B ligand (RANKL), it was identified as the key mediator of osteoclastogenesis, [41] its presence is associated to bone control regeneration and remodeling; sclerostin (SOST), SOST mRNA is expressed in many tissues especially during embryogenesis, during bone remodeling sclerostin prevent activation of osteoblasts and bone formation without previous bone resorption [42]; basic fibroblast growth factor-2 (FGF-2), it is synthesized and secreted by human adipocytes and act increasing pre-osteoblasts proliferation [43].

Fig. 6 shows that all transcription factors related to osteogenic commitment are expressed during hASCs differentiation in the presence of HA-nanostructured network cultured in a non-osteogenic media since the first 7 days of treatment, and that the obtained values are in general statistically comparable to those obtained under the influence of soluble osteogenic additives (C+). The obtained results reaffirm our previously acquired conclusion related to the material's ability to induce *per se* an osteogenic behavior. There is a specific materials' influence on selected gene expressions subject to culture media conditions and the temporal evolution of the differentiation process. At the initial 7 days of treatment the materials' presence induces in cDMEM a superior expression of ALPL, COL1A1, OPG and SOST genes with respect to C+. A meaningful effect is appreciated for COL1A1 and SOST on the MI and MII dry-coatings respectively. After 21 days of treatment, RUNX2, OC, OSX, OPN, BMP2, FGF2, RANKL and SOST were down regulated; with an important effect on OSX and RANKL in the presence of MI, Fig. 7.

Osteonectin, ALPL, COL1A1 and OPG were up regulated regardless of the material's nature, Fig. 7. The presence of an osteogenic culture

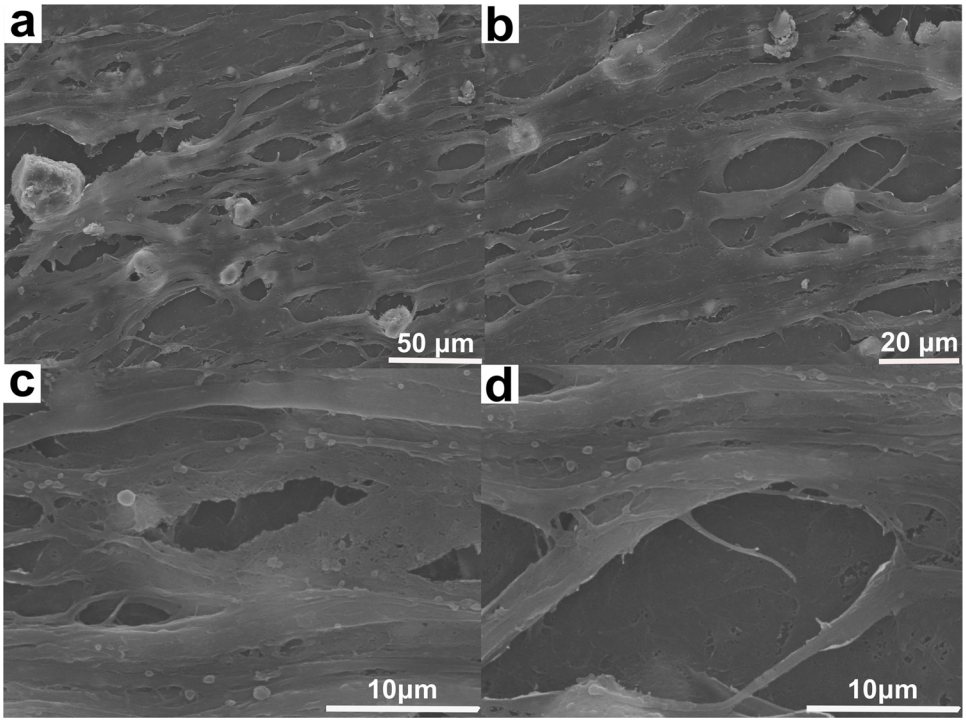

Fig. 5. SEM microphotographs of hASCs adhered on 60 µg/cm^2 nanostructured MII dry-coating cultured throughout 21 days in ODM.

media does not mask the effect of the materials on the differentiation process. At the 7 days of treatment and, despite the presence of osteogenic soluble additives in the culture medium, OPN y OSX were down regulated noticing the superiority of the material effect on the osteogenic additives. Likewise, ALPL, COL1A1, RANKL and SOST were up regulated with a greater effect of MI dry-coating, Fig. 6. After 21 days of treatment, there was a statistically significant decrease respect to C + of OSX, OPN, BMP2, RANKL and SOST's expression. However, the ALPL and COL1A1 levels were up regulated Fig. 7.

5. Discussion

Niches are local tissue microenvironments that maintain and regulate stem cells activation; [5] a synthetic material that carefully mimics human osteogenic niches represents a successfully address thought bone-bioreactors conceptions. In this work we determine the aptitude of nanostructure enriched HA-frameworks to support the anchorage, subsistence and osteogenic commitment of hASCs; results are contrasted with those attained by the application of a standard cocktail for osteogenic differentiation of multipotent stem cells: dexamethasone (Dex), ascorbic acid (AA) and β-glycerophosphate (β-Gly) [44]. Both materials increased the mitochondrial metabolic activity (MMA) and proliferation of hASC in cDMEM, Fig. 1**a–e**, nevertheless, after 21 days of treatments, the presence of MII leads to statistically comparable values to that achieved under ODM culture, Fig. 1**e**. Alizarin Red S test and APL activity revealed a clear substrate stimulus exerted by nanostructure HA-framework dry-coatings on the osteogenic differentiation potential of hASCs from the initial 7 days of culture that is considerably increased after 21 days of treatment; for a second time MII evidenced a superior influence, Figs. 2 and 3. The maintenance and survival of hASCs is strongly influenced by local microenvironment stimuli, including the material's surface roughness and morphology (in short its nano-topography). [45] Emergent evidence has revealed that nano-topography participate in the overall control of stem cells (SCs) fate [45,46] and that its boost is equivalent to the exerted by genetic and molecular mediators. [44,46] According to their roughness parameters, **Fig. SI11**, both MI and MII material exhibit submicron surface roughness with an asymmetrical outward as a result of HA nano-rods aggregation, [9,10] resembling the natural ECM dimension, which contains pits, pores and protrusions in the length scale of 5–200 nm. [47] Analysis of optical and SEM microphotographs, Figs. 3–5, revealed a pronounced material-cellular interaction both in cDMEM and ODM, however such interaction is different in each culture media. After 21 days of cultured in cDMEM cells extend, organize and distribute around HA substrate displaying actin stress fibers and focal adhesions clusters, as shown by its well-defined star morphology characteristic of high-tension states. [45] On the other hand, cells cultured in ODM shows signs of increased motility, as indicated by their elongated morphology paralleled oriented. [48] The magnitude of the spreading area positively correlate with the cellular proliferation activity in the initial phase of cell dissemination; [49] in agreement, the high cellular spreading on the materials dry-coatings reveled by optical and SEM microscopy, Figs. 3–5, is coherent with the observed increase of viability and MMA values, Fig. 1. The obtained results are in completely agreement to literature findings that point out that substrates displaying submicron surface roughness influence cells orientation and contact guidance as their dimensions are comparable to cell filopodia sizes (50–100 nm) [47,50]. The superior effect displayed by MII sample could be related to its irregular peak's and valley's size distribution [10]. Studies performed by Dalby et al. [51] revealed that there is an increase of osteoprogenitor cells adhesion onto disorder and asymmetrical nano-topographies. We think that an analogous effect takes place when hADSCs spread onto MII dry-coating in our experimental conditions.

In anchorage-dependent cells, as the hASCs, adhesion plays a number of roles in the discrete cell functions, including the differentiation stage where adhesion-derived tension is a key point. It is generally accepted that surfaces stimulating higher adhesion and spreading are implicated in hard-tissue (bone/osteoblast) phenotypes development [45]. Results of ALP activity test after 21 days of treatment displayed very large values of ALP activity for hASCs spread on HA-frameworks dry-coatings cultured in cDMEM compared with its counterparts cultured in ODM, Fig. 2. Alizarin Red S assays, meanwhile, shows an increase of cellular motility and proliferation in ODM, Fig. 3.

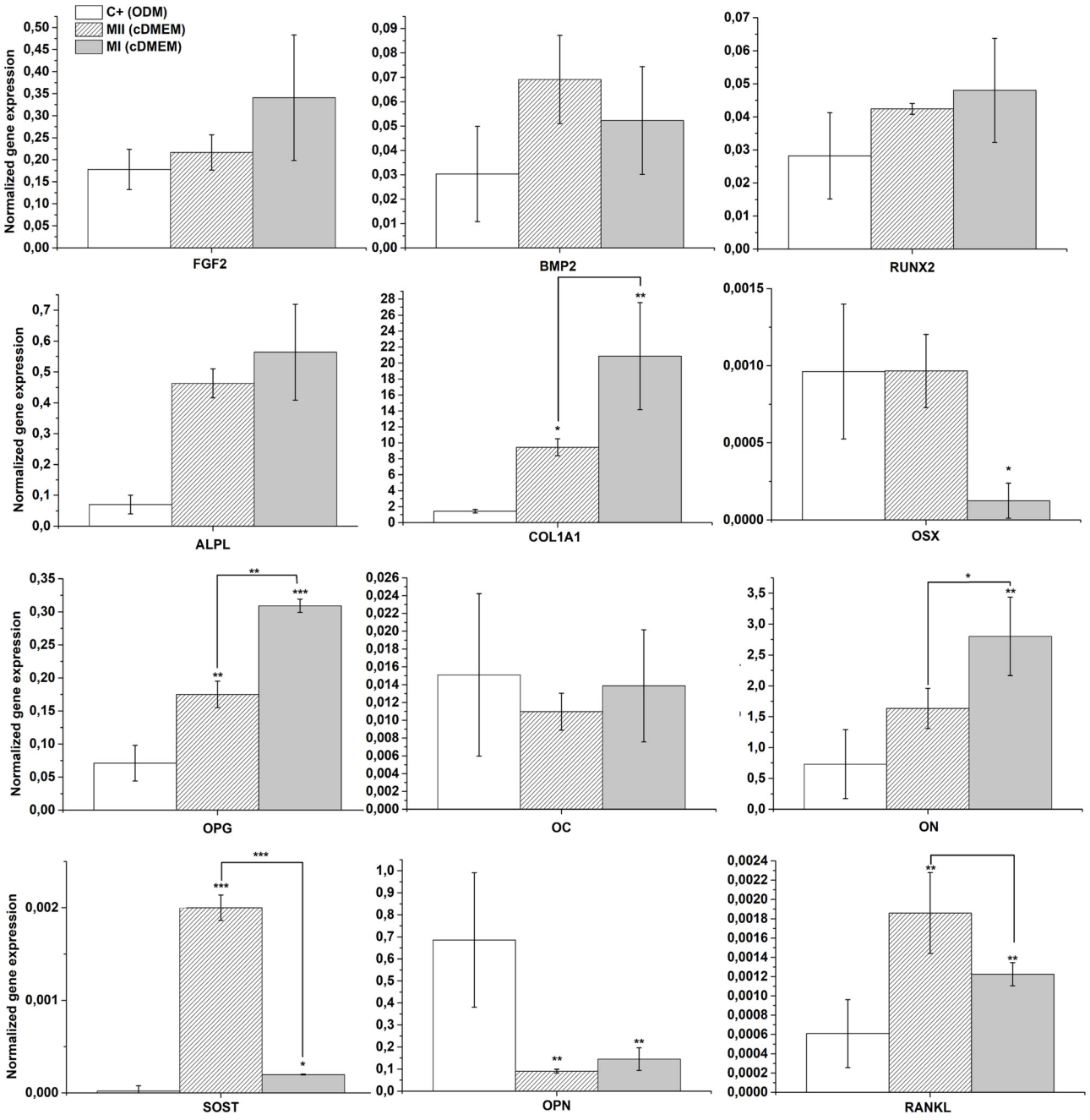

Fig. 6. Analysis of gene expressions involved in osteogenic commitment. The effect of HA-frameworks on hASCs exposed to either osteogenic (ODM) and non-osteogenic (cDMEM) media throughout 7 days are compared. Data are normalized to housekeeping gene (TFRC). Cells cultured in ODM on uncoated wells were used as control (C+). Asterisks denote statistically significant differences (*$p < 0.05$, **$p < 0.01$ and ***$p < 0.001$). Significant differences between the samples are indicated with brackets.

There is not a linear dependence between cell spreading and cell proliferation; the increased spreading, formation of adhesion units and assembly of the actin cytoskeleton provoke cell proliferation only to a certain degree [49]. Literature results propose that the proliferation capacity and migration speed of various cell types, including SCs, cultivated on several substrates is highest at intermediate adhesion strength, while high adhesion capacity is reasonably associated with quiescence and maturation stages of cells [49]. This literature information support our obtained results, the superior cellular attachment attained over the HA dry-coatings in cDMEM involve a slower cell proliferation but a higher maturation than the provided by soluble osteogenic additives. The lesser maturation reached in ODM conditions implies lower ALP activity values, as well as a reduced mineralization, such as those obtained in our results. Foundations of this effect could be originated in the mechanism of cells-substrate anchorage. It is accepted that cell spreading stimulates cell proliferation and differentiation by biochemical and mechanical pathways [45,49,51]. Both mechanisms start by the adsorption of cell adhesion-mediating molecules (*i.e.*, vitronectin and fibronectin proteins, among others [52]) in a precise configuration from biological fluids *in vivo* and from FBS *in vitro* to the material surface. Then the active sites in these adsorbed molecules bond to cell adhesion receptors, which involve integrin and non-integrin (*i.e.*, proteoglycan-based) adhesion molecules [49]. Previously obtained results [10] indicated that water molecules adsorbs on HA substrate, in those moderately hydrophobic conditions adhesive proteins from serum would adsorb in a flexible and adjustable form where the oligopeptidic

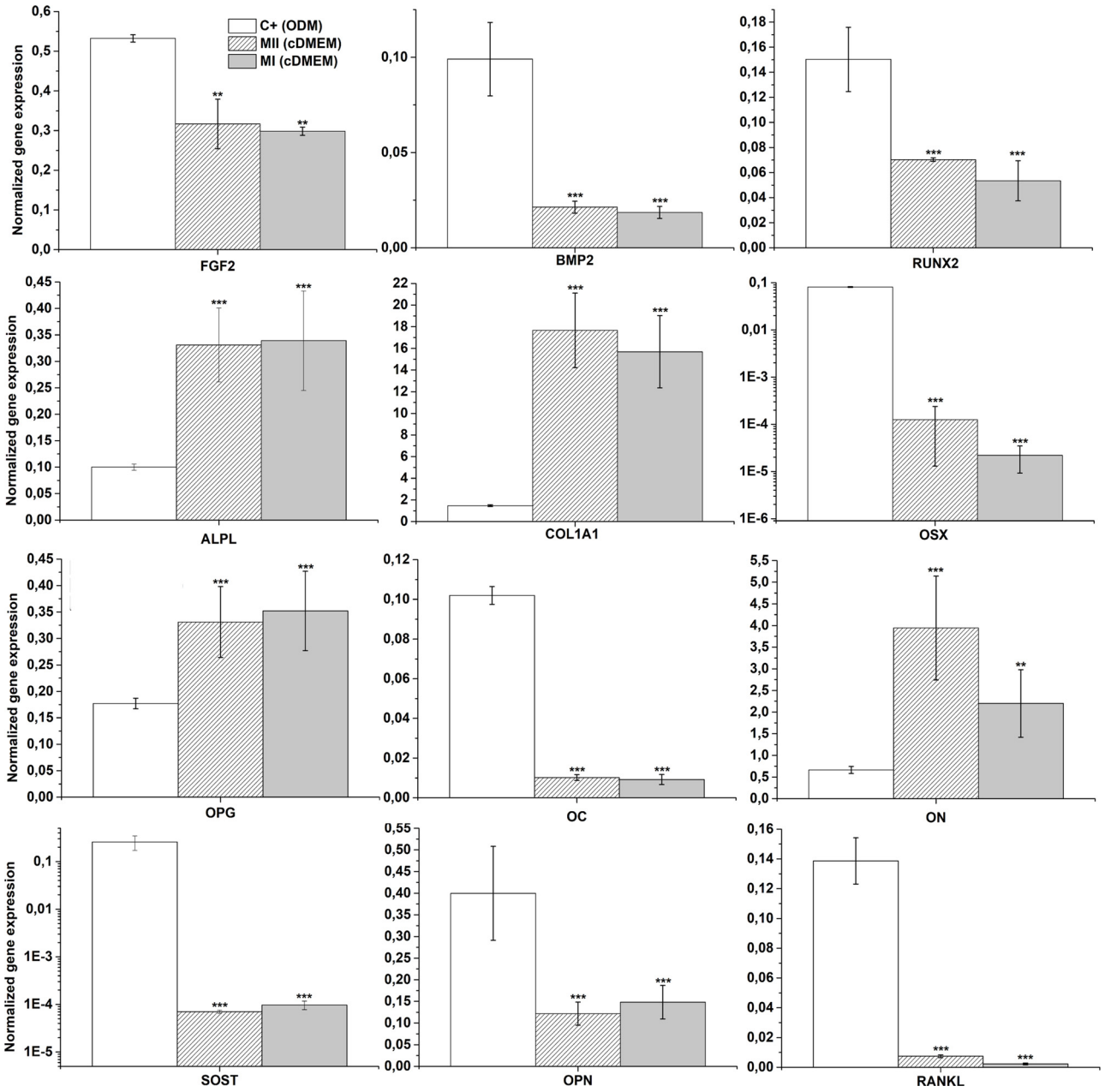

Fig. 7. Analysis of gene expressions involved in osteogenic commitment. The effect of HA-frameworks on hASCs exposed to either osteogenic (ODM) and non-osteogenic (cDMEM) media throughout 21 days are compared. Data are normalized to housekeeping gene (TFRC). Cells cultured in ODM on uncoated wells were used as control (C+). Asterisks denote statistically significant differences (*$p < 0.05$, **$p < 0.01$ and ***$p < 0.001$). Significant differences between the samples are indicated with brackets.

ligands acquired a loop-like conformation accessible to the pocket-like structure of adhesion receptors [49]. We assume that this process favorably occurs in cDMEM, while in ODM the presence of soluble additives (Dex, AA, β-Gly) compete and interfere with the adsorption of FBS's proteins. Analyzing the molecular formula of the components of ODM, it can be seen that their chemical structure include a large number of hydroxyl groups (−OH), those can strongly adsorb on Ca^{2+} positions of HA crystals' surfaces that act as Lewis acid sites [53]. In addition, being smaller in size than proteins, they diffuse faster to the material's surface limiting the adsorption active sites. With not enough protein molecules adsorbed on HA-frameworks dry-coatings, there is a transitional cell adhesion that favors cellular motility and proliferation but a lesser maturation.

Concerning to the regulation of gene expression profile, Scheme 1, the transcriptional activation of selected genes on hASCs spread out on HA-frameworks dry-coatings in cDMEM was consistent with osteogenic commitment; ALPL, COL1A1, OPG, SOST expressions are up regulated compared to ODM conditions. The obtained results reveal that RUNX2 and OSX, which are positive transcriptional regulators of genes like COL1A1, OC, ON, and OPN [54], are completely modulated during osteogenesis with a distinctive expression profile, Figs. 6 and 7. At first 7 days of treatment, expressions of RUNX2 and OSX have no statistically differences to ODM conditions, while their levels decreased in the next 21 days. The complex interplay between RUNX2 and OSX is obviously reflected on the modulation of target genes during different phases of differentiation. While OSX activation during osteoblast formation contributes to OPG early activation, its following decrease is known to be required to promote osteoblast differentiation at late stage in a RUNX2 independent manner [55]. On the other hand, the initial high levels of RUNX2 are coherent with its role in the sequential

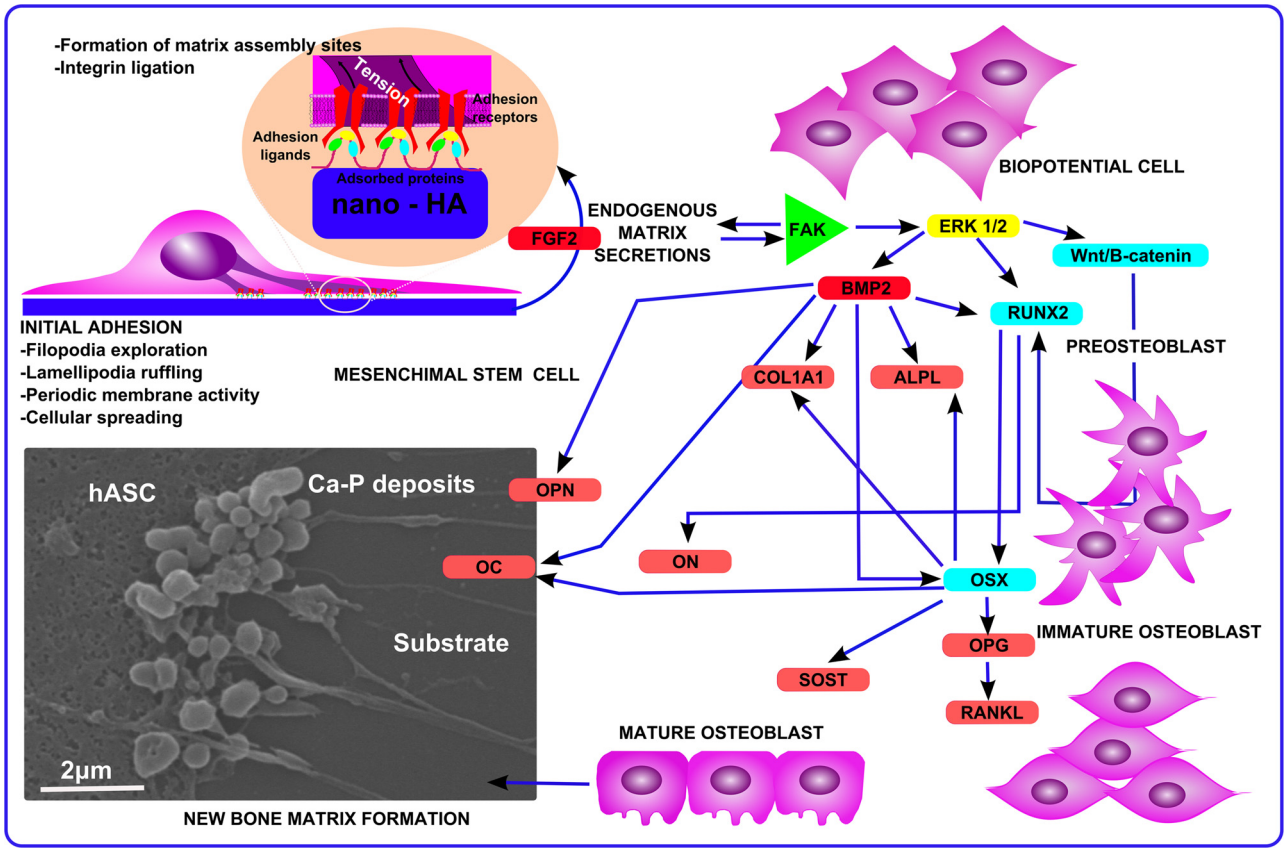

Scheme 1. Putative mechanism of signaling pathway governing hASCs osteogenic commitment under HA-nanostructured framework substrate stimuli after 7 days of culture in cDMEM. Initial adhesion stimulates endogenous secretions and FGF2 expression [59]. FGF2 affect integrin activity on the surface by initiating conformational changes that expose ligand binding sites [59]. Upon integrin ligation, focal adhesion kinase (FAK) is activated. Through the integrin-dependent translocation of extracellular signaling-related kinase 1 and 2 (ERK 1/2) pathways, FAK mediates expression of target genes BMP2, RUNX2 [56] and Wnt. [60] RUNX2 commits hASCs towards osteogenic lineage and inhibits adipogenic differentiation. After commitment, hASCs differentiated into preosteoblasts which express RUNX2 and high levels of COL1A1 and ALPL. Preosteoblasts differentiate into immature osteoblasts that express BMP2, OSX, β-catenin, bone matrix proteins, OPN and develop into mature osteoblasts. Mature osteoblasts express OC, ALPL and COL1A1; neogenesis of mineralized matrix.

activation of COL1A1, ALPL and OC, which are involved in intermediate and later stages of matrix maturation and bone mineralization. The activation of BMP2, FGF2, ALPL, COL1A1, OC, and OPN that play a role in cell adhesion, proliferation, extracellular matrix maturation and differentiation of the osteoblast phenotype [32,34,37,38,39,43], showed that cell proliferation and progression through cell cycle induced by the HA-nanostructured frameworks are fast and deliberately from the initial stages of treatment. Down-regulation of RUNX2 and OSX after 21 days of treatment seemed to be associate in a direct manner with focal adhesion maturation, indicating the involvement of ERK 1/2 negative feedback pathways following integrin-mediated FAK activation [56].

In addition of FAK→ ERK ½ pathway, in the presence of Ca-P materials, selected gene expression routes could be stimulated by Ca^{2+} or PO_4^{3-} ions that could be a consequence of the substrate degradation, **Fig. SI12**. As an example, OPN levels have a direct response to increased PO_4^{3-} concentrations [57] and, the effects of BMP2 on OC, RUNX2 and OSX expressions can be enhanced by an increase of extracellular Ca^{2+} concentration [58,59]. In our case, OPN expression is down regulated whenever the cells were cultured on HA-nanostructured dry-coatings in cDMEM or in ODM. Regarding BMP2, OC, RUNX2 and OSX levels, the material exerts a down regulation respect to C+ after 21 days of treatment. These facts indicate that in our experimental conditions the presence of extracellular Ca^{2+} and PO_4^{-3} ions are not the main mechanism of gene regulation and confirms the importance of the nanotopography to regulate cellular adhesion and their subsequent fate. Moreover, the distinctive temporal regulation of OPG/RANKL system and SOST, functionally linked to bone remodeling, [35,41,42] suggest the capacity of the HA-nanostructure substrate to support the tightly coupled processes of bone resorption and formation, allowing a wave of bone formation to follow each cycle of bone resorption, thus maintaining skeletal integrity and potentiality to act as bone niche.

Summarizing, HA-frameworks dry coatings provide a slower growing of hASCs than soluble osteogenic additives but promote a better adhesion and a fast osteogenic maturation.

6. Conclusion

Here we showed the ability of nanostructured HA-frameworks dry-coatings to direct hASCs' osteogenic fate in a non-osteogenic differentiation media and, that the interaction of cell´s focal adhesion on materials surfaces provides a superior effect to those reached under the influence of osteogenic soluble additives: dexamethasone (Dex), ascorbic acid (AA) and β-glycerophosphate (β-Gly). It was demonstrated that the transcriptional activation of selected genes on hASCs cultured in the presence of HA-frameworks dry-coatings are completely modulated with a distinctive osteogenic expression profile leading to the adequate temporal evolution of the successive stages of bone regeneration: proliferation, differentiation and maturation. The observed differences in gene expression profiles might be related to an overall enhanced protein adsorption on HA-nanostructured materials and the activation of FAK → ERK ½ pathways. Considering the two tested materials, a better performance was attained by one of them exhibiting

less regular peak's and valley's size distribution topography.

The obtained results highlight the importance of nanotopography in the stem cells fate regulation and validate the potential of hASCs - nanostructured HA-frameworks systems to act as bone bioreactors. As mentioned previously, topography in the nanoscale range is capable to significant influence the amount and functionality of protein adsorbed on biomaterials surfaces. This hypothesis, however, deserves further investigation involving analysis of specific regulatory and structural proteins; which are already part of our future work.

Conflicts of interest

There are no conflicts of interest to declare.

Acknowledgements

The authors acknowledge Universidad Nacional del Sur (PGI 24/Q064), Concejo Nacional de Investigaciones Científicas y Técnicas de la República (CONICET, PIP – 11220130100100CO), Agencia Nacional de Promoción Científica y Tecnológica (ANPCyT, PICT 201-0126), Argentina and the ERASMUS MUNDUS – AMIDILA program. JS has doctoral fellowship of CONICET. PVM is an independent researcher of CONICET.

Appendix A. Supplementary data

Supplementary material related to this article can be found, in the online version, at doi:https://doi.org/10.1016/j.mtcomm.2018.05.010.

References

[1] A.R. Amini, C.T. Laurencin, S.P. Nukavarapu, Bone tissue engineering: recent advances and challenges, CRC Crit. Rev. Bioeng. 40 (2012) 363–408.
[2] R. Dimitriou, E. Jones, D. McGonagle, P.V. Giannoudis, Bone regeneration: current concepts and future directions, BMC Med. 9 (2011) 66.
[3] M.M. Stevens, R.P. Marini, D. Schaefer, J. Aronson, R. Langer, V.P. Shastri, In vivo engineering of organs: the bone bioreactor, Proc. Natl. Acad. Sci. U. S. A. 102 (2005) 11450–11455.
[4] J.M. Benyus, Biomimicry, William Morrow Paperbacks, New York, 1997.
[5] S.J. Morrison, D.T. Scadden, Nature 505 (2014) 327–334.
[6] T. Gong, J. Xie, J. Liao, T. Zhang, S. Lin, Y. Lin, Nanomaterials and bone regeneration, Bone Res. 3 (2015) 15029.
[7] G.G. Walmsley, A. McArdle, R. Tevlin, A. Momeni, D. Atashroo, M.S. Hu, A.H. Feroze, V.W. Wong, P.H. Lorenz, M.T. Longaker, D.C. Wan, Nanotechnology in Bone Tissue Engineering, Nanomedicine 11 (2015) 1253–1263.
[8] Q. Wang, J. Yan, J. Yang, B. Li, Mater. Today 19 (2016) 451–463.
[9] N.L. D'Elía, A.N. Gravina, J.M. Ruso, J.A. Laiuppa, G.E. Santillán, P.V. Messina, Biophys. Acta Gen. Subj. 1830 (2013) 5014–5026.
[10] N.L. D'Elia, C. Mathieu, C.D. Hoemann, J.A. Laiuppa, G.E. Santillan, P.V. Messina, Nanoscale 7 (2015) 18751–18762.
[11] A. Contreras-Garcia, D. Maxime, N.L. D'Elía, C.-H. Lafantaisie-Favreau, J.C. Ruiz, G.-E. Rivard, W. Michel, P. Messina, C.D. Hoemann, Montréal, Canada, May, Presented in Part at Front. Bioeng. Biotechnol. Conference (2016).
[12] G.T.A. Salazar, O. Ohneda, Biophys. Rev. 5 (2013) 11–28.
[13] R. Dai, Z. Wang, R. Samanipour, K.-i. Koo, K. Kim, Stem Cells Int. 2016 (2016) 19.
[14] S.-P. Huang, C.-H. Huang, J.-F. Shyu, H.-S. Lee, S.-G. Chen, J.Y.-H. Chan, S.-M. Huang, J. Biomed. Sci. 20 (2013) 51.
[15] Y.S. Choi, G.J. Dusting, S. Stubbs, S. Arunothayaraj, X.L. Han, P. Collas, W.A. Morrison, R.J. Dilley, J. Cell. Mol. Med. 14 (2010) 878–889.
[16] H. Tapp, E.N. Hanley, J.C. Patt, H.E. Gruber, Exp. Biol. Med. 234 (2009) 1–9.
[17] M. Tobita, H. Mizuno, Int. J. Oral Maxillofac. Implants 28 (2013) e487–e493.
[18] D.A. Banyard, A.A. Salibian, A.D. Widgerow, G.R. Evans, J. Cell. Mol. Med. 19 (2015) 21–30.
[19] A. Pozzuoli, C. Gardin, R. Aldegheri, E. Bressan, M. Isola, J. Calvo-Guirado, C. Biz, P. Arrigoni, L. Ferroni, B. Zavan, J. Osseointegr. 8 (2016) 2–7.
[20] Z. Ding, Z. Fan, X. Huang, Q. Lu, W. Xu, D.L. Kaplan, ACS Appl. Mater. Interfaces 8 (2016) 24463–24470.
[21] G. Kaur, M.T. Valarmathi, J.D. Potts, E. Jabbari, T. Sabo-Attwood, Q. Wang, Biomaterials 31 (2010) 1732–1741.
[22] F. Denizot, R. Lang, J. Immunol. Methods 89 (1986) 271–277.
[23] N.J. Marshall, C.J. Goodwin, S.J. Holt, Growth Regul. 5 (1995) 69–84.
[24] T.L. Riss, R.A. Moravec, A.L. Niles, S. Duellman, H.A. Benink, T.J. Worzella, L. Minor, et al., Assay guidance manual, in: G.S. Sittampalam, N.P. Coussens, K. Brimacombe (Eds.), Eli Lilly & Company and the National Center for Advancing Translational Sciences, Cell Viability Assays, Bethesda (MD), 2004[Internet]. Available from: http://www.ncbi.nlm.nih.gov/books/NBK144065/.
[25] E.R. Fischer, B.T. Hansen, V. Nair, F.H. Hoyt, D.W. Dorward, Current Protocols in Microbiology Chap 2, (2012) Unit2B.2.
[26] M.W. Pfaffl, Nucleic Acids Res. 29 (2001) e45.
[27] J.M. Ruso, J. Sartuqui, V.P. Messina, Curr. Top. Med. Chem. 15 (2015) 2290–2305.
[28] P. Janicki, G. Schmidmaier, Injury 42 (2011) S77–S81.
[29] H.-J. Prins, A.K. Braat, D. Gawlitta, W.J.A. Dhert, D.A. Egan, E. Tijssen-Slump, H. Yuan, P.J. Coffer, H. Rozemuller, A.C. Martens, Stem Cell Res. 12 (2014) 428–440.
[30] E.E. Golub, K. Boesze-Battaglia, Curr. Opin. Orthop. 18 (2007) 444–448.
[31] J. Lian, C. Stewart, E. Puchacz, S. Mackowiak, V. Shalhoub, D. Collart, G. Zambetti, G. Stein, Proc. Natl. Acad. Sci. U. S. A. 86 (1989) 1143–1147.
[32] H.-M. Ryoo, H.M. Hoffmann, T. Beumer, B. Frenkel, D.A. Towler, G.S. Stein, J.L. Stein, A.J. Van Wijnen, J.B. Lian, Mol. Endocrinol. 11 (1997) 1681–1694.
[33] J.D. Termine, H.K. Kleinman, S.W. Whitson, K.M. Conn, M.L. McGarvey, G.R. Martin, Cell 26 (1981) 99–105.
[34] F.P. Reinholt, K. Hultenby, A. Oldberg, D. Heinegård, Proc. Natl. Acad. Sci. U. S. A. 87 (1990) 4473–4475.
[35] N. Udagawa, N. Takahashi, H. Yasuda, A. Mizuno, K. Itoh, Y. Ueno, T. Shinki, M.T. Gillespie, T.J. Martin, K. Higashio, Endocrinology 141 (2000) 3478–3484.
[36] T. Koga, Y. Matsui, M. Asagiri, T. Kodama, B. de Crombrugghe, K. Nakashima, H. Takayanagi, Nat. Med. 11 (2005) 880–885.
[37] S. Gronthos, A.C. Zannettino, S.E. Graves, S. Ohta, S.J. Hay, P.J. Simmons, J. Bone Min. Res. 14 (1999) 47–56.
[38] R. Cancedda, Curr. Pharm. Des. 15 (2009) 1334–1348.
[39] J. Yang, P. Shi, M. Tu, Y. Wang, M. Liu, F. Fan, M. Du, Food Sci. Hum. Wellness 3 (2014) 127–135.
[40] M.-a. Milona, J.E. Gough, A.J. Edgar, BMC Genom. 4 (2003) 43–54.
[41] S. Khosla, Endocrinology 142 (2001) 5050–5055.
[42] M. Moester, S. Papapoulos, C. Löwik, R. Van Bezooijen, Calcif. Tissue Int. 87 (2010) 99–107.
[43] M.C. Kühn, H.S. Willenberg, M. Schott, C. Papewalis, U. Stumpf, S. Flohé, W.A. Scherbaum, S. Schinner, Mol. Cell. Endocrinol. 349 (2012) 180–188.
[44] F. Langenbach, J. Handschel, Stem Cell Res. Ther. 4 (2013) 117.
[45] M.J. Dalby, N. Gadegaard, R.O.C. Oreffo, Nat. Mater. 13m (2014) 558–569.
[46] E. Bressan, A. Carraro, L. Ferroni, C. Gardin, L. Sbricoli, R. Guazzo, E. Stellini, M. Roman, P. Pinton, S. Sivolella, Nanomedicine 8 (2013) 469–486.
[47] M.S. Lord, M. Foss, F. Besenbacher, Nano Today 5 (2010) 66–78.
[48] S. Foldberg, M. Petersen, P. Fojan, L. Gurevich, T. Fink, C.P. Pennisi, V. Zachar, Colloids Surf. B. 93 (2012) 92–99.
[49] L. Bacakova, E. Filova, M. Parizek, T. Ruml, V. Svorcik, Biotechnol. Adv. 29 (2011) 739–767.
[50] M.O. Riehle, M.J. Dalby, H. Johnstone, A. MacIntosh, S. Affrossman, Mater. Sci. Eng., C. 23 (2003) 337–340.
[51] M.J. Dalby, N. Gadegaard, R. Tare, A. Andar, M.O. Riehle, P. Herzyk, C.D.W. Wilkinson, R.O.C. Oreffo, Nat. Mater. 6 (2007) 997–1003.
[52] K.M. Hennessy, W.C. Clem, M.C. Phipps, A.A. Sawyer, F.M. Shaikh, S.L. Bellis, Biomaterials 29 (2008) 3075–3083.
[53] V. Bolis, C. Busco, G. Martra, L. Bertinetti, Y. Sakhno, P. Ugliengo, F. Chiatti, M. Corno, N. Roveri, Philos. Trans. R. Soc. A. 370 (2012) 1313–1336.
[54] P. Ducy, C. Desbois, B. Boyce, G. Pinero, B. Story, C. Dunstan, E. Smith, J. Bonadio, S. Goldstein, C. Gundberg, A. Bradley, G. Karsenty, Nature 382 (1996) 448–452.
[55] C.A. Yoshida, H. Komori, Z. Maruyama, T. Miyazaki, K. Kawasaki, T. Furuichi, R. Fukuyama, M. Mori, K. Yamana, K. Nakamura, PLoS One 7 (2012) e32364.
[56] J.W. Cassidy, J.N. Roberts, C.-A. Smith, M. Robertson, K. White, M.J. Biggs, R.O.C. Oreffo, M.J. Dalby, Acta Biomater. 10 (2014) 651–660.
[57] G.R. Beck, B. Zerler, E. Moran, Proc. Natl. Acad. Sci. U. S. A. 97 (2000) 8352–8357.
[58] R. Aquino-Martínez, N. Artigas, B. Gámez, J.L. Rosa, F. Ventura, PLoS One 12 (2017) e0178158.
[59] M.I. Kokkinos, H.J. Brown, R.U. de Iongh, Mol. Vis. 13 (2007) 418–430.
[60] J. Du, Y. Zu, J. Li, S. Du, Y. Xu, L. Zhang, L. Jiang, Z. Wang, S. Chien, C. Yang, Sci. Rep. 6 (2016) 203951-12.